

## RESEARCH ARTICLE

# A Miniaturized High-Gain Multi-Beam Lens Antenna Based on Quasi-Conformal Transformation Optics

MIAO LV<sup>1,2</sup>, LI ZHANG<sup>1,2</sup>, MENGYI LI<sup>1</sup>, FANCHAO ZENG<sup>1,3</sup>, (Graduate Student Member, IEEE), SHAOLI ZUO<sup>1</sup>, ZHI-YA ZHANG<sup>1,4</sup>, YU WANG<sup>2,4</sup>, AND TONG WU<sup>1</sup>

<sup>1</sup>National Key Laboratory of Radar Detection and Sensing, Xi'an 710071, China

<sup>2</sup>The 20th Research Institute of China Electronics Technology Group Corporation, Xi'an 710068, China

<sup>3</sup>Global Big Data Technologies Centre (GBDTC), University of Technology Sydney (UTS), Sydney, NSW 2007, Australia

<sup>4</sup>CETC Key Laboratory of Data Link Technology, Xi'an 710068, China

Corresponding authors: Zhi-Ya Zhang (zyzhang@xidian.edu.cn) and Fanchao Zeng (Fanchao.zeng@student.uts.edu.au)


This work was supported in part by the National Natural Science Foundation of China under Grant 62271372; and in part by the Key Laboratory of Data Link Technology, China Electronics Technology Group Corporation, under Grant CLDL-20202413.

**ABSTRACT** This paper presents the design of a novel multi-beam Luneburg lens antenna with specific dielectric structure and proposes a new solution for downsizing planar lens antennas. The quasi-conformal transformation optics (QCTO) principle is applied to achieve an equivalent transformation relation between the spatial coordinate and the electromagnetic properties of material, effectively preserving the behavior of electromagnetic waves while achieving a significant reduction in antenna size. The antenna comprises a deformed Luneburg lens with a radius equivalent to  $3.75\lambda$ , metal plates flanking the lens, and a linear array of seven microstrip antennas operating at 10 GHz. By selectively activating antenna elements within the array, the antenna can generate seven distinct beams, enabling a scanning range of  $\pm 30^\circ$  in the azimuth plane. Each beam achieves a gain exceeding 15 dBi. In comparison to traditional planar lens antennas, this antenna boasts a reduction in size of more than 30% and has the flexibility of being fed using a linear array.

**INDEX TERMS** High gain, Luneburg lens, multibeam antenna, miniaturization, quasi-conformal transformation optics (QCTO), 3D printing.

## I. INTRODUCTION

In the realm of modern passive radar detection, and mobile communication systems, the ability to concurrently detect and track multiple targets, or to execute multi-beam scanning, is paramount [1]. Addressing these needs typically involves two main technologies: electronically controlled phased array antennas [2], [3] and mechanically controlled reflector antenna systems [4]. Electronically controllable phased array antennas are known for their effectiveness but are often hindered by their complexity and substantial cost. Conversely, mechanically scanning reflector antenna systems, although a viable alternative, face operational difficulties, limited rotation speed, and elevated maintenance

The associate editor coordinating the review of this manuscript and approving it for publication was Shah Nawaz Burokur .

expenses. As a practical alternative to the aforementioned antennas, lens antennas with gradient refractive index, such as Luneburg lens antennas, are commonly employed in the field. These lens antennas provide a more practical and cost-effective solution, ensuring efficient operation in various communication systems. Fig. 1 illustrates the application scenario of a multi-beam antenna.

The Luneburg lens, introduced in 1944 by physicist Luneburg and detailed in his book “The Mathematical Theory of Optics” [5], represents a pivotal advancement in spherical lens technology. Characterized by its gradient refractive index and geometric axisymmetry, the Luneburg lens is renowned for its exceptional beam focusing capabilities. It uniquely converges incident waves from any direction on its surface and efficiently transforms spherical waves emanating from or near a point on its sphere into plane waves.



**FIGURE 1.** Example of utilizing a multi-beam antenna.

These characteristics enable Luneburg lens antennas to excel in multi-beam applications.

However, the non-uniform distribution of lens materials poses a challenge to their fabrication. To address this challenge, various processing techniques have been employed, such as foam compression [6], [7], [8], radial drilling on dielectric materials [9], [10], and notably, 3D printing technology. 3D printing technology stands out for its advantages of flexible structure, high processing accuracy, and rapid integration, making it particularly suitable for manufacturing complex structures [11], [12], [13], [14], [15], [16]. In previous research, a lens model was formed by utilizing a substrate consisting of multiple dielectric plates with varying relative dielectric constants, achieving a relative dielectric constant range from 1.1 to 7.8 [17]. However, the assembly process of different dielectrics may introduce gaps or bonding materials, potentially impacting the antenna's performance. Alternatively, a study [18] successfully 3D printed a lens with a periodic honeycomb structure using ceramic material and demonstrated an increased gain of over 5 dB when paired with a standard gain horn antenna.

In addition to fabrication challenges, lens antennas often face issues with efficiency and gain reduction. To address this issue, a deformed Luneburg lens was developed. The deformed lens alters its shape and dielectric constant based on the principles of transformation optics theory, resulting in attributes such as high directivity, low sidelobe levels, and wide beam coverage. Furthermore, it offers advantages including high aperture efficiency, convenient loading, and ease of conformation [19], [20], [21]. The concept of an elliptical Luneburg lens was first introduced with the design of a six-layer ellipsoidal lens, revealing that optimal antenna performance is attained when the distance between the source and the lens is roughly equivalent to the wavelength [22]. Further research showed that a hemispherical Luneburg lens, when paired with a reflector, could achieve performance comparable to a full spherical lens, underscoring the effectiveness of hemispherical designs [23].

The traditional spherical Luneburg lenses are often too large for practical applications, prompting researchers to seek ways to miniaturize them. While alternative shapes such as

ellipsoidal and hemispherical lenses have been explored, they still result in relatively large antennas. This ongoing challenge has steered the development towards more compact planar Luneburg lenses [24], [25]. Key innovations in this area include manipulating the machine radius of the electrolyte column between parallel waveguide plates [26]. A notable advancement involved a design using air, E-shaped microstrip patch antennas, parallel plates, and epoxy resin piles to create a cylindrical lens antenna that mimics the dielectric constant distribution of a Luneburg lens [27]. Additionally, there has been research into using cost-effective polymers like polystyrene to replicate the gradient index in cylindrical lens antennas between parallel plates [28], [29], [30].

While both the Gutman lens and the traditional Luneburg lens are alternatives for lens design, the Gutman lens differs in terms of its more compact size [31]. Previous research has demonstrated that Gutman's excitation source allows for movement within a smaller focal circle, which results in a reduction in antenna size. However, current studies on the Gutman lens primarily focus on its three-dimensional characteristics [32], [33]. Although truncated Gutman lenses have been explored to decrease the size of the lens antenna, challenges remain in reducing the size for two-dimensional scanning applications. Luneburg lenses have garnered more attention than Gutman lenses in the design of lens antennas for two-dimensional applications.

In [34], an innovative approach was taken to modify the spherical Luneburg lens using Quasi-conformal transformation optics (QCTO), effectively deforming its bottom into a plane. This modification addressed the challenges in arranging lens antenna sources, a notable inconvenience in antenna source processing. Furthermore, based on the space filling curve, the lens was processed by FDM fusion laminating 3D printing technology [33]. Following this development, a wideband anti-reflection layer was introduced [35]. This additional design significantly alleviated the impedance mismatch caused by the QCTO deformation, subsequently reducing the half-power beamwidth of the lens antenna. It is evident that these modifications were aimed at addressing the inconveniences associated with the arrangement of the antenna sources, ultimately leading to improved performance.

In this work, a novel multi-beam Luneburg lens antenna with compact size, high gain and high efficiency is proposed. The QCTO theory is employed to achieve a size reduction of over 30% for the lens. The microstructure of the medium material designed by equivalent medium theory is used to determine the material properties of the ideal antenna model. Additionally, 3D printing technology is applied in the design, facilitating the fabrication. The proposed multi-beam lens antenna is fabricated, measured, and compared with state-of-the-art designs. The comparison shows that the proposed antenna exhibits compact size, higher gain and efficiency, which serves as an excellent candidate for point-to-point communication, wireless communication and mobile communication.

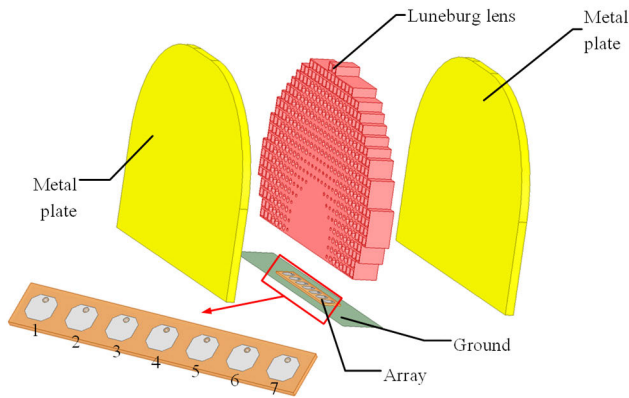


FIGURE 2. Configuration of the developed multi-beam Luneburg lens antenna.

The main contributions that we describe in this paper are as follows. Our work takes a holistic approach, optimizing the shaping method, modifying the dielectric constant distribution, utilizing 3D printing for fabrication, to enhance the overall performance and make it more practical for real-world applications. More importantly, instead of using a conformal array to feed the lens antenna, the proposed compact Luneburg lens antenna features simple linear feeding array for multi-beam and high gain application.

II. DESIGN PRINCIPLE OF THE TRANSFORMED LUNEBURG LENS ANTENNA

Fig. 2 illustrates the proposed lens antenna design, which consists of three main components: a linear feed antenna array, a modified planar Luneburg lens with an optimized structure, and two metal plates. The feed, designed as a microstrip antenna, is strategically placed beneath the lens. The lens itself, based on a planar Luneburg design, has been miniaturized and deformed using the QCTO principle to attain the necessary relative dielectric constant, implemented via the equivalent medium method. A detailed analysis of this antenna will be presented in the following sections.

A. LENS MINIATURIZATION BY QCTO THEORY

The QCTO theory is derived from the transformation optics (TO) theory, which is used to address the electromagnetic properties of the medium in physical space and determine the expected electromagnetic wave path. Fig. 3(a) displays the cross-sectional outline of the planar Luneburg lens, representing the virtual space before transformation. This space is mesh-divided using the Cartesian coordinate system for detailed analysis. The transformation process aims to create a physical space that accommodates specific design needs, including at least one straight edge to facilitate the circular-arc distribution focus of the planar Luneburg lens. As a result, the transformed physical space features the lens contour and grid division as illustrated in Fig. 3(b). In the transformation process, an arc line located at the bottom of the outer contour of the lens in the virtual space shown in

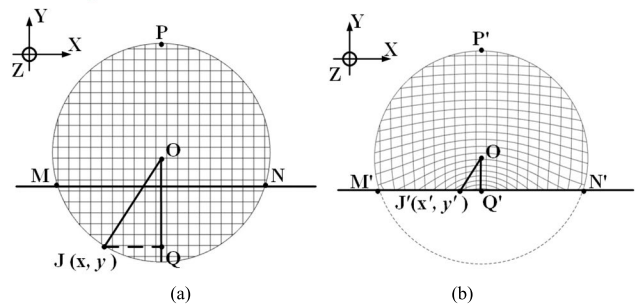


FIGURE 3. The transformation of the lens contour and grid segmentation in (a) virtual space, and (b) physical space.

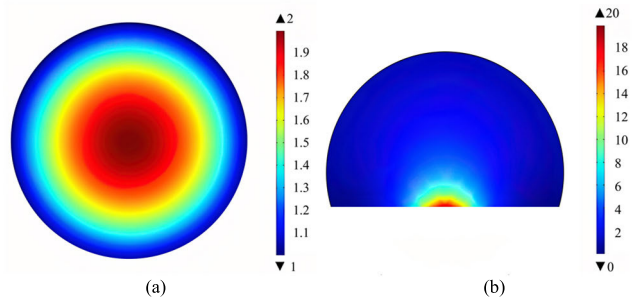
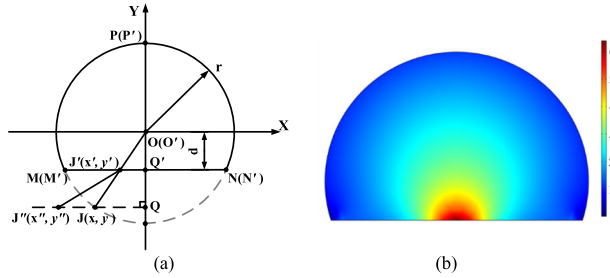


FIGURE 4. Dielectric constant distribution of lens in different space. (a) Virtual space. (b) Physical space.

Fig. 3(a) is selected. After fixing its two endpoints, M and N, the arc is extruded inward until it is finally transformed into a straight-line segment M'Q'N' in Fig. 3(b).

The process of determining the dielectric constant of a lens is conducted in COMSOL by simulating the ideal Luneburg lens in virtual space. By determining the electromagnetic wave transmission path, the boundary conditions during the deformation process of the lens are established based on the approximate orthogonality of the lens grid in the deformed physical space. By solving the Laplace equation, the relative dielectric constant distribution of the deformed lenses can be determined. The lens mesh in the transformed space remains quasi-orthogonal, aligning with QCTO theory as evidenced in Fig. 3. Nevertheless, the deformed lens configuration is incompatible with the Neumann boundary condition, thereby necessitating the implementation of the Dirichlet boundary condition to effectively solve the problem. To facilitate this, the horizontal and vertical coordinates are directly assigned to the transformed boundary by utilizing the coordinate mapping relationship between the corresponding points on the model boundary before and after transformation. Defining the radius of the planar Luneburg lens in virtual space as  $r$ , and the vertical distance between the bottom edge of the deformed lens and the center of the circle in physical space as  $d$ , the transformation segment of the outer contour of the lens can be denoted by the straight-line segment M'N'. In Fig. 3, any point on the lower arc is denoted by J, with its corresponding point in physical space as J'. If the coordinates of J are  $(x, y)$ , the coordinates of J' are  $(x', y')$ , and Q and Q' represent the



**FIGURE 5.** The modification of (a) coordinate mapping of model transformation, and (b) dielectric constant distribution.

perpendicular feet of  $J$  and  $J'$  on the  $Y$ -axis respectively. Then, through a geometric analysis, the following relations (1) can be derived:

$$\begin{cases} x|_{MPN} = x' \\ x|_{MN} = \frac{r \cdot x'}{\sqrt{x'^2 + d^2}} \end{cases} \begin{cases} y|_{MPN} = y' \\ y|_{MN} = \frac{r \cdot y'}{\sqrt{x'^2 + d^2}} \end{cases} \quad (1)$$

The radius  $r$  of the planar Luneburg lens antenna plays a pivotal role in determining the antenna's size and, consequently, its gain. Larger apertures generally yield improved gain but may suffer from reduced aperture efficiency when overly large. In this design, the deformable lens in physical space is compressed at its base, resulting in a smaller vertical distance  $d$  and a reduced antenna aperture. This transformation leads to a decrease in feed antenna gain. Balancing the requirements of feed dimensions, operating frequency, and gain, the radius  $r$  of the antenna is optimized at 112.5 mm, with the vertical distance  $d$  set to 37.5 mm.

Fig. 4(a) shows the relative permittivity of a planar Luneburg lens in virtual space, with a central value of 2 tapering to 1 at the circumference, indicating a gradual permittivity change. Conversely, Fig. 4(b) displays the relative dielectric constant of the deformed lens in physical space, where the transformation process introduces several notable issues in the dielectric constant distribution. As shown in Fig. 4(b), the QCTO transformation leads to a relative dielectric constant in the deformed lens ranging from 0 to 20, with areas exhibiting excessively high values, posing challenges in lens fabrication and practical implementation. Additionally, a significant portion of the lens shows a dielectric constant near 1, similar to air, reducing its effective area and impacting antenna performance. These issues highlight the need for further optimization and adjustment of the transformation process to improve the lens's functionality.

The high dielectric constant in the deformed lens predominantly occurs near the center of its bottom, with the highest value around the midpoint of the bottom-line segment. This value gradually decreases radiating from the midpoint. To address this, modifications in the coordinate mapping relationship pre- and post-QCTO transformation are required, along with adjustments to the Dirichlet boundary conditions and the coordinate mapping formula. A practical solution involves further stretching the boundary coordinates of the virtual space along the  $X$ -axis, as illustrated in Fig. 5(a).

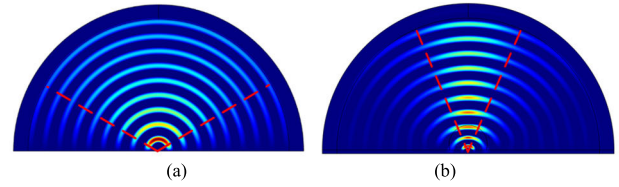


**FIGURE 6.** The propagation of electromagnetic waves (a) without lens, and (b) with lens.

In this figure, the adjusted point in the virtual space is marked as  $J''(x'', y'')$ . While the ordinate mapping remains constant, the abscissa mapping range is expanded to accommodate these changes and mitigate issues related to the high dielectric constant distribution.

$$x''|_{MN} = Ax' \quad y''|_{MN} = y|_{MN} = \frac{r \cdot y'}{\sqrt{x'^2 + d^2}} \quad (2)$$

where  $A$  is a constant, its value must satisfy the formula,  $|x''| > |x|$ , so the range of  $A$  is:

$$A > \frac{r}{\sqrt{x'^2 + d^2}} > \frac{r}{\sqrt{r^2 + d^2}} \quad (3)$$

The optimal dielectric constant distribution of the lens, as depicted in Fig. 5(b), was determined using the values of radius  $r$  and vertical distance  $d$  in equation (3), resulting in a parameter  $A > 0.955$ . To refine the lens model, a value of  $A = 1.07$  was employed. Any region of the lens with a dielectric constant less than 1 was considered equivalent to air, given that the relative permittivity of air is 1. Consequently, in the deformed lens design, segments with a relative permittivity below 1 were disregarded and treated as air.

Fig. 6 illustrates the E-field distribution both with and without the lens. In Fig. 6(a), the absence of the lens results in a divergent E-field spread across a wide angle, indicative of a broader beam with lower gain. Conversely, with the lens incorporated, as shown in the subsequent panel, the E-field concentrates into a narrower angle, yielding a tighter beam with increased gain. The comparison between the behaviors of the electromagnetic waves before and after the addition of the lens clearly reveals the lens' capacity to concentrate the waves, thus demonstrating its convergence effect. Consequently, the ability of Luneburg lenses to enhance the antenna's gain becomes evident.

## B. DIELECTRIC CONSTANT LAYERING AND PUNCHING

Layering and punching methods are typically used to create the dielectric constant profile for a Luneburg lens. Following the adjustment of boundary conditions, the deformed lens achieves a relative dielectric constant ranging from 1 to 6.3, with only a minor area exceeding 3. This distribution is advantageous for the feed antenna's irradiation and subsequent processing. To ensure the lens antenna's performance and minimize issues during the splicing of different media, a single-substrate material 3D printing method is preferred.

After evaluating various options, DSM-8000 is selected as the raw material for 3D printing due to its stable dielectric

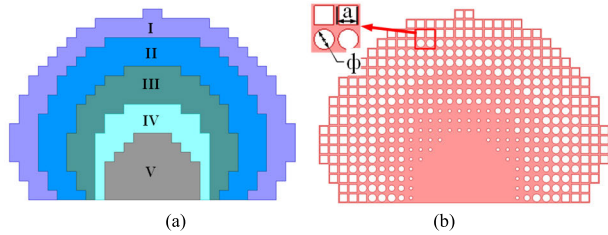


FIGURE 7. (a) Simplified lens model. (b) The hole punching structure of the deformed Luneburg lens.

TABLE 1. Parameters of the luneburg lens.

Region	$\epsilon_r$	Duty Cycle	Hole Diameter / Side Length(mm)
I	1.25	83.26%	$a=6.8$
II	1.75	55.12%	$\phi=6.28$
III	2.25	31.21%	$\phi=4.73$
IV	2.75	9.93%	$\phi=2.67$
V	3	\	\

constant of around 3 in the operating frequency band. This selection leads to a simplification of the designed lens model. The resulting lens, depicted in Fig. 7(a), benefits from a small span and high stability. The dielectric constants of the lens material, from the outermost to the innermost of the five layers, are set at 1.25, 1.75, 2.25, 2.75, and 3, respectively, aligning with the lens’s dielectric constant distribution requirements. While increasing the number of layers theoretically improves the fidelity to the original dielectric constant distribution, it also complicates manufacturing and assembly processes. Conversely, reducing the number of layers simplifies production but at the expense of antenna performance. This presents a critical balance between performance optimization and manufacturing feasibility.

The entire lens is segmented into five layers, and areas of the deformed lens with a relative dielectric constant above 3 are treated as equivalent to 3 for simplicity. Our simulation results indicate that this equivalence has a small impact on the lens antenna’s performance while significantly decreasing the selection and processing of lens materials. To ease the processing, the dimensions of each discrete small element are increased to 7.5 mm × 7.5 mm. The duty cycle of these elements is calculated based on the equivalent medium theory, using a dielectric constant of 3 for the substrate and 1 for inserted air, leading to the design of a square hole structure.

Fig. 7(b) illustrates the punching structure and structural parameters of the deformable Luneburg lens. Due to the relatively low dielectric constant of the outermost layer, most of the deformed lenses utilize a circular hole structure. However, this structure cannot achieve the required duty cycle for a single element. Therefore, specific parameter values for the structure are detailed in Table 1, with the code for each lens area referenced according to Fig. 7(a). This approach facilitates the practical realization of the lens while maintaining the desired dielectric properties.

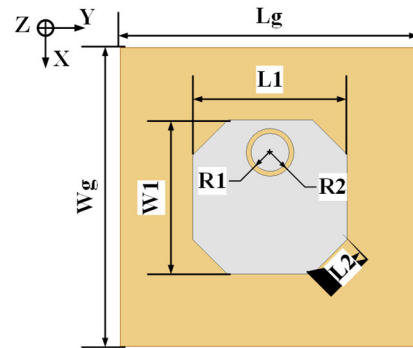


FIGURE 8. The structure of feeding antenna element. ( $W_g = 15$  mm,  $L_g = 15$  mm,  $L_1 = 9$  mm,  $W_1 = 9$  mm,  $R_1 = 0.75$  mm,  $R_2 = 0.95$  mm,  $L_2 = 3$  mm.)

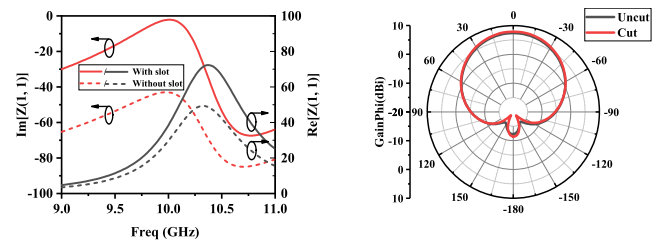
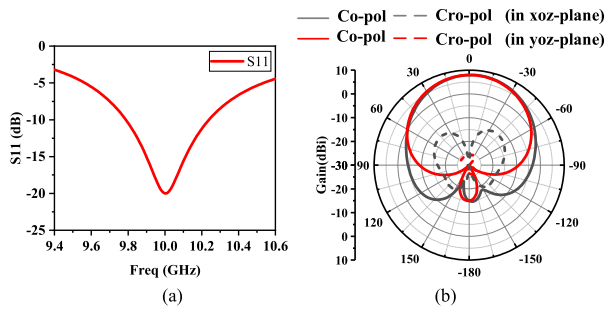


FIGURE 9. Comparison of (a) impedance between the patch with slot and without slot and (b) gain between the cut corner patch and the uncut corner patch.

### C. FEEDING ANTENNA ELEMENT DESIGN

In the design of a miniaturized multi-beam lens antenna, the choice of feed antennas is crucial, particularly considering the need for smaller dimensions and higher gain. As shown in Fig. 8, a miniaturized microstrip patch antenna is selected as the feeder for the antenna. The patch antennas are printed on Rogers 5880 substrate, which has a dielectric constant ( $\epsilon_r$ ) of 2.2 and a loss tangent ( $\tan \delta$ ) of 0.0009. The thickness of this substrate is 1.5 mm.

The deformed Luneburg lens antenna is fed by a basic microstrip antenna selected as the feed source. The patch shape of the upper layer is square, and the antenna is fed by the coaxial line. The feed point is designed at the center of the square radiation patch to align with the vertical linear polarization mode of the antenna. This antenna’s design represents a notable divergence from conventional coaxial line-fed microstrip patch antennas. It innovatively incorporates a ring slot around the feeding point on the radiation patch. By introducing a circular patch coupled feeding method through a circular slot surrounding the feeding point of the antenna, the antenna’s feeding mechanism transitions from direct feeding to circular patch coupling feeding within the slot. This structural modification, as shown in Fig. 9(a), significantly increases the antenna’s capacitance, balancing the inductive component introduced by the feeding probe and facilitating impedance matching. Additionally, through simulation analysis, it was discovered that chamfering the corners of the microstrip patch slightly enhances the antenna’s gain,



**FIGURE 10.** (a) The simulated reflection coefficient and (b) radiation pattern at 10GHz of the antenna element.

as depicted in Fig. 9(b). The gain of the chamfered antenna is nearly identical in size to the unchamfered microstrip patch. The chamfering was chosen to further enhance the gain performance of the lens antenna, aiming for high gain capabilities in the antenna design.

The simulated results of the patch antenna are presented in Fig. 10. Fig. 10(a) illustrates the S11 parameter, which remains below  $-10$  dB in the frequency range of 9.72 GHz to 10.32 GHz, indicating efficient impedance matching. Additionally, Fig. 10(b) showcases the antenna's symmetrical radiation pattern at 10 GHz in both E and H planes, characterized by low cross-polarization and relatively high gain. These results underline the antenna's optimized design, achieving a balance between size reduction and high-performance metrics. Finally, the feed array consists of seven optimized patch antennas, which are used for multi-beam scanning by feeding each element one by one.

#### D. THE OPTIMIZATION OF THE LENS ANTENNA

After completing the equivalent structural design of the deformed Luneburg lens, the next step involves conducting extensive simulations to assess the performance of the Luneburg multi-beam lens antenna. Especially, it's crucial to determine two key parameters: the thickness ( $W$ ) of the deformed Luneburg lens and the focal length ( $H$ ) from the lens's bottom to the feed antenna array. These parameters are pivotal as they significantly influence the antenna system's overall performance and operational capabilities.

Utilizing QCTO theory and compressing the volume of a flat Luneburg lens results in the focal point shifting outward at the bottom of the deformed lens. To address this, a width ( $W$ ) of 26 mm was initially chosen for the lens. For analysis, only the center element was activated. Due to the focal points of cylindrical Luneburg lenses being distributed along the side of the lens, rather than at any point on the surface like traditional spherical Luneburg lenses, we hypothesize that altering the shape may impact the distribution of the focal points. Therefore, we adjusted the position of the lens above the feed array to find the optimal placement for the array. By adjusting the vertical distance between the feed element's phase center and the lens's bottom edge to simulate antenna radiation pattern at various feed heights ( $H$ ) at the center

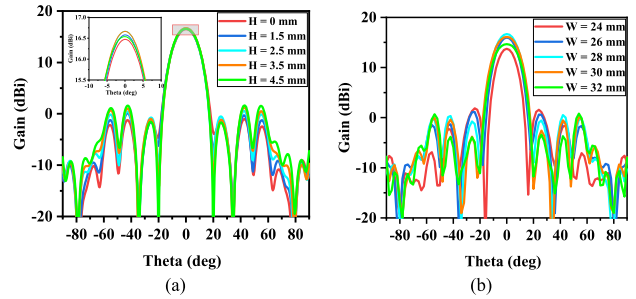


**FIGURE 11.** The simulated radiation pattern comparison with (a) different feed heights  $H$  and (b) different thickness  $W$ .

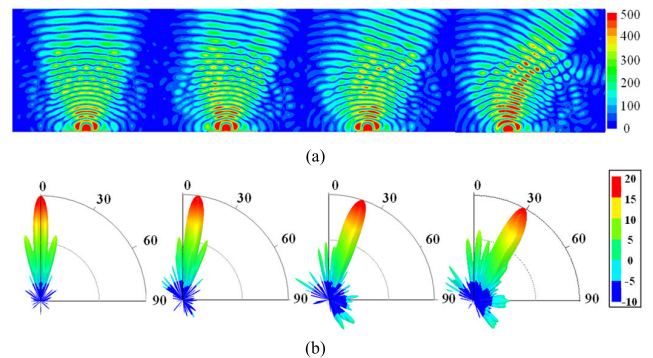


**FIGURE 12.** (a) Simulated E-field distribution, and (b) corresponding 3D radiation pattern with different scanning angles.

frequency of 10GHz, as shown in Fig. 11(a). As the lens height increases, so do the gain and sidelobe level of the antenna. Eventually, a height of  $H = 3.5$  mm was selected to achieve higher gain and lower sidelobes.

What's more, the width ( $W$ ) of the deformed Luneburg lens was then optimized. When selecting the lens width, it is important to ensure it is not too small to cover the entire array. Therefore, we chose 26mm as the initial width for the lens. Antenna radiation pattern for different lens widths ( $W$ ) is generated at the center frequency of 10GHz, as depicted in Fig. 11(b). The antenna gain initially increases with lens width, then decreases, peaking at  $W = 28$  mm, where the sidelobe level is also low. Consequently,  $W = 28$  mm was established as the final width parameter, striking an optimal balance between gain enhancement and sidelobe reduction.

Finally, the optimized lens antenna is analyzed under full wave simulation, Fig. 12 illustrates the electric field distribution and beam performance of the lens antenna operating at 10GHz. Fig. 12(a) clearly demonstrates the simulated E-field distribution when different ports are activated. This simulation vividly captures how the lens consolidates electromagnetic fields, channeling them into a scanning beam. Correspondingly, Fig. 12(b) displays the 3D radiation patterns corresponding to E-field distribution, demonstrating the antenna's ability to maintain a well-defined directional beam at varying angles, indicative of its high-performance multi-beam capabilities.

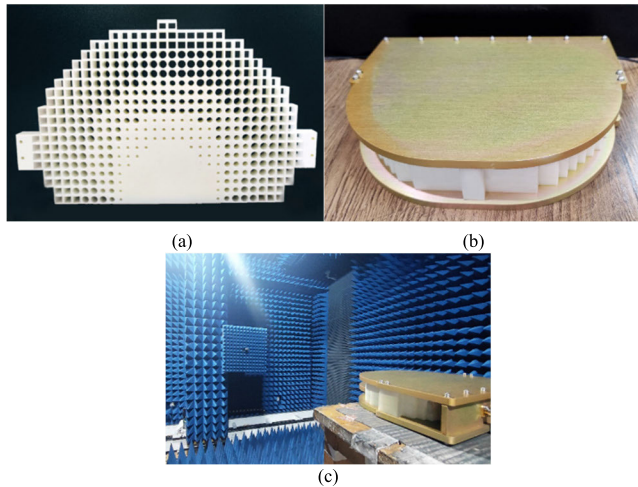


FIGURE 13. The prototype of (a) single lens and (b) lens antenna. (c) Testing environment.

III. EXPERIMENTAL RESULTS

The fabrication and measurement of the proposed lens antenna are illustrated in Fig. 13. The lens is fabricated using a 3D printing technique, the metal plate and ground are produced through Computer Numerical Control (CNC) machining, and the antenna module is created using the Printed Circuit Board (PCB) method. Fig. 13(a) presents the 3D-printed lens, distinguished by its array of varying holes. The assembled prototype, complete with the feeding array, is depicted in Fig. 13(b). Fig. 13(c) showcases the performance evaluation of the antenna, conducted in an anechoic chamber. The simulation and measurement results of the reflection coefficients when exciting a single antenna element are plotted in Fig. 14 (a). In general, the measured and simulated results agree well with each other. As shown in Fig. 14(a), the measured bandwidth of all ports can cover the bandwidth of 9.8 GHz - 10.2 GHz. In Fig. 14(b), the simulated and measured radiation patterns of all seven beams operating at 10GHz are depicted, all of which are directional and closely resemble the simulation results. Despite a slight reduction in the measured beam gain, the antenna successfully obtained a scanning range of  $\pm 30^\circ$ .

Fig. 15 displays the isolation between feeding units and the aperture efficiency at 10 GHz, as determined through simulation and measurement. As illustrated in Fig. 15(a), we present both the simulated and measured port isolations between different ports. Due to the symmetrical structure of the antenna array, the isolation for the first half of the ports is displayed. It can be observed that all isolations exceed 17 dB. Fig. 15(b) shows the performance of the simulated and measured aperture efficiency of the lens antenna. It can be seen from the figure that the proposed antenna achieves high efficiency, exceeding 57%-71% within the working frequency bandwidth. Furthermore, the test results are in good agreement with the simulation results, confirming the reliability and performance of our design.

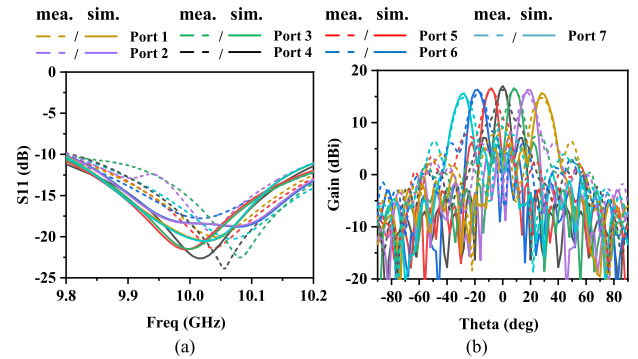


FIGURE 14. Simulated and measured (a) S11 parameters of seven ports and (b) scanning radiation pattern.

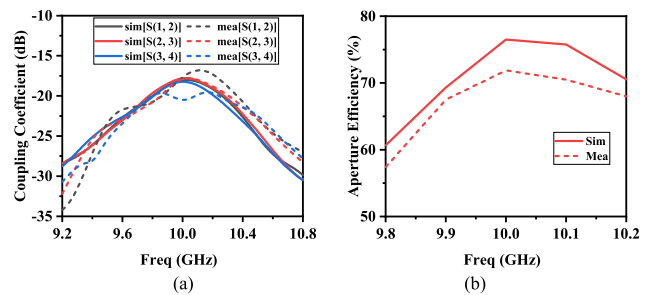


FIGURE 15. (a) Coupling coefficient between different ports and (b) simulated and measured aperture efficiency of lens antenna.

TABLE 2. Comparison with the existing similar lens antenna.

Ref.	Frequency	Gain	Sweep angle	Size(r)	aperture efficiency	Whether the feed array is linear
[16]	28GHz	>12dBi	$\pm 30^\circ$	$4.66\lambda$	66%	Yes
[22]	79.5GHz	>19dBi	$83^\circ$	$6.37\lambda$	63%	No
[23]	30GHz	>13dBi	$\pm 67^\circ$	$5\lambda$	30%	No
[24]	60GHz	>18dBi	$52^\circ$	$5.6\lambda$	$\approx 60\%$	No
[33]	12.5GHz	>20dBi	$\pm 40^\circ$	$6.25\lambda$	\	No
[38]	12.5GHz	>29dBi	$\pm 15^\circ$	$6.35\lambda$	$\approx 60\%$	No
[39]	31.75GHz	>19dBi	$\pm 44^\circ$	$5\lambda$	46%-85%	No
[40]	60GHz	>20dBi	$\pm 12^\circ$	$5\lambda$	31.8%	Yes
[41]	10GHz	\	$\pm 24^\circ$	\	\	No
[42]	16GHz	>12.8dBi	$\pm 25^\circ$	$>4.26\lambda$	\	No
This work	10GHz	>15dBi	$\pm 30^\circ$	$3.75\lambda$	57%-71%	Yes

A comparison with existing state-of-the-art lens antennas is illustrated in Table 2. The lens antenna developed in this work is distinguished by its substantially reduced radius, making it more compact than previous designs. Importantly, this reduction in size does not detract from its performance; the proposed design ensures both high gain and high efficiency. Even among lenses of comparable size, this antenna is noteworthy, particularly for its capability to operate with a linear feed—a versatile feature well-regarded across various applications. The compactness and functionality are a direct result of applying the QCTO principle, which involved

reshaping the lens to achieve a smaller, more efficient antenna size.

#### IV. CONCLUSION

A multi-beam high-gain Luneburg lens antenna is proposed in this paper. It operates at a frequency of 10GHz, relies on a unique dielectric structure to achieve a remarkable scanning range of  $\pm 30^\circ$  in the azimuth plane, generating seven beams, each surpassing a gain of 15dBi. The innovative dielectric structure implemented in this antenna design not only reduces its volume by more than 30% when compared to conventional planar Luneburg lens antennas but also enables seamless integration with a linearly arranged feed array. These capabilities make the lens suitable for various applications such as point-to-point communication, 5G remote coverage and mobile communication.

#### REFERENCES

- [1] G. C. Tavik, C. L. Hilterbrick, J. B. Evins, J. J. Alter, J. G. Crnkovich, J. W. de Graaf, W. Habicht, G. P. Hrin, S. A. Lessin, D. C. Wu, and S. M. Hagewood, "The advanced multifunction RF concept," *IEEE Trans. Microwave Theory Techn.*, vol. 53, no. 3, pp. 1009–1020, Mar. 2005, doi: [10.1109/TMTT.2005.843485](https://doi.org/10.1109/TMTT.2005.843485).
- [2] L. Xi, S. Zhidong, and W. Shuai, "Design of T/R module for air-borne ultra-wideband phased array radar," *Chin. J. Radio Sci.*, vol. 1, no. 2, pp. 264–269, 2020.
- [3] M.-C. Tang, S. Xiao, B. Wang, J. Guan, and T. Deng, "Improved performance of a microstrip phased array using broadband and ultra-low-loss metamaterial slabs," *IEEE Antennas Propag. Mag.*, vol. 53, no. 6, pp. 31–41, Dec. 2011, doi: [10.1109/MAP.2011.6157712](https://doi.org/10.1109/MAP.2011.6157712).
- [4] O. Manoochehri, A. Emadeddin, A. Darvazehban, and D. Erricolo, "A new method for designing high efficiency multi feed multi beam reflector antennas," in *Proc. Int. Conf. Electromagn. Adv. Appl.*, Sep. 2017, pp. 551–554, doi: [10.1109/ICEAA.2017.8065304](https://doi.org/10.1109/ICEAA.2017.8065304).
- [5] R. K. Luneburg, *The Mathematical Theory of Optics*. Providence, RI, USA: Brown University Press, 1944.
- [6] G. D. M. Peeler and H. P. Coleman, "Microwave stepped-index Luneburg lenses," *IRE Trans. Antennas Propag.*, vol. 6, no. 2, pp. 202–207, 1958.
- [7] J. Bor, O. Lafond, B. Fuchs, H. Merlet, P. Le Bars, and M. Himdi, "Light and cheap flat foam-based Luneburg lens antenna," in *Proc. 8th Eur. Conf. Antennas Propag.*, Apr. 2014, pp. 3200–3204.
- [8] J. Bor, O. Lafond, M. Himdi, H. Merlet, and P. Lebars, "Smooth plate Luneburg lens with superstrate," in *Proc. 9th Eur. Conf. Antennas Propag.*, Apr. 2015, pp. 1–4.
- [9] K. A. Zimmerman and D. L. Runyon, "Luneburg lens and method of constructing same," U.S. Patent 5 677 796 A, Aug. 25, 1995.
- [10] K. Sato and H. Ujiie, "A plate Luneburg lens with the permittivity distribution controlled by hole density," *Electron. Commun. Jpn. Part I, Commun.*, vol. 85, no. 9, pp. 1–12, Sep. 2002.
- [11] Z. Larimore, S. Jensen, A. Good, A. Lu, J. Suarez, and M. Mirotznik, "Additive manufacturing of Luneburg lens antennas using space-filling curves and fused filament fabrication," *IEEE Trans. Antennas Propag.*, vol. 66, no. 6, pp. 2818–2827, Jun. 2018.
- [12] M. Liang, W.-R. Ng, K. Chang, K. Gbele, M. E. Gehm, and H. Xin, "A 3-D Luneburg lens antenna fabricated by polymer jetting rapid prototyping," *IEEE Trans. Antennas Propag.*, vol. 62, no. 4, pp. 1799–1807, Apr. 2014.
- [13] Z. W. Chen, Z. Y. Li, J. J. Li, C. B. Liu, C. S. Lao, Y. L. Fu, C. Y. Liu, Y. Li, P. Wang, and Y. He, "3D printing of ceramics: A review," *J. Eur. Ceram. Soc.*, vol. 39, no. 4, pp. 661–687, 2019.
- [14] H. Hassanin, K. Essa, A. Elshaer, M. Imbaby, H. H. El-Mongy, and T. A. El-Sayed, "Micro-fabrication of ceramics: Additive manufacturing and conventional technologies," *J. Adv. Ceram.*, vol. 10, no. 1, pp. 1–27, Feb. 2021, doi: [10.1007/s40145-020-0422-5](https://doi.org/10.1007/s40145-020-0422-5).
- [15] J. Oliveira, V. Correia, H. Castro, P. Martins, and S. Lanceros-Mendez, "Polymer-based smart materials by printing technologies: Improving application and integration," *Additive Manuf.*, vol. 21, pp. 269–283, May 2018.
- [16] K. Liu, S. Yang, S. Qu, Y. Chen, and J. Hu, "2D flat Luneburg lens antenna for multibeam scanning application," *Electron. Lett.*, vol. 55, no. 25, pp. 1317–1318, Dec. 2019, doi: [10.1049/el.2019.2901](https://doi.org/10.1049/el.2019.2901).
- [17] J. G. Marin and J. Hesselbarth, "Lens antenna with planar focal surface for wide-angle beam-steering application," *IEEE Trans. Antennas Propag.*, vol. 67, no. 4, pp. 2757–2762, Apr. 2019.
- [18] F. Wang, Z. Li, Y. Lou, F. Zeng, M. Hao, W. Lei, X. Wang, X. Wang, G. Fan, and W. Lu, "Stereolithographic additive manufacturing of Luneburg lens using Al<sub>2</sub>O<sub>3</sub>-based low sintering temperature ceramics for 5G MIMO antenna," *Additive Manuf.*, vol. 47, Nov. 2021, Art. no. 102244.
- [19] J. B. Pendry, D. Schurig, and D. R. Smith, "Controlling electromagnetic fields," *Science*, vol. 312, no. 5781, pp. 1780–1782, Jun. 2006.
- [20] U. Leonhardt, "Optical conformal mapping," *Science*, vol. 312, no. 5781, pp. 1777–1780, Jun. 2006.
- [21] J. Li and J. B. Pendry, "Hiding under the carpet: A new strategy for cloaking," *Phys. Rev. Lett.*, vol. 101, no. 20, Nov. 2008, Art. no. 203901.
- [22] A. Demetriadou and Y. Hao, "Slim Luneburg lens for antenna applications," *Opt. Exp.*, vol. 19, no. 21, p. 19925, 2011.
- [23] J. Thornton, "Wide-scanning multi-layer hemisphere lens antenna for Ka band," *IEE Microwave Antennas Propag.*, vol. 153, no. 6, p. 573, 2006.
- [24] Z. Shi, S. Yang, S. W. Qu, and Y. Chen, "Circularly polarised planar Luneburg lens antenna for mm-wave wireless communication," *Electron. Letters*, vol. 52, no. 15, pp. 1281–1282, 2016.
- [25] S. S. Vinnakota, R. Kumari, H. Meena, and B. Majumder, "Rectifier integrated multibeam Luneburg lens employing artificial dielectric as a wireless power transfer medium at mm wave band," *IEEE Photon. J.*, vol. 13, no. 3, pp. 1–14, Jun. 2021, doi: [10.1109/JPHOT.2021.3079180](https://doi.org/10.1109/JPHOT.2021.3079180).
- [26] C. Wang, J. Wu, and Y.-X. Guo, "A 3-D-Printed wideband circularly polarized parallel-plate Luneburg lens antenna," *IEEE Trans. Antennas Propag.*, vol. 68, no. 6, pp. 4944–4949, Jun. 2020.
- [27] K. Liu, S. Yang, Q. Jiang, and S.-W. Qu, "A lightweight multi-beam cylindrical Luneburg lens antenna loaded with multiple dielectric posts," *Int. J. RF Microwave Comput.-Aided Eng.*, vol. 29, no. 1, Jan. 2019, Art. no. e21511.
- [28] X. Wu and J.-J. Laurin, "Fan-beam millimeter-wave antenna design based on the cylindrical Luneberg lens," *IEEE Trans. Antennas Propag.*, vol. 55, no. 8, pp. 2147–2156, Aug. 2007.
- [29] C. Hua, N. Yang, X. Wu, and W. Wu, "Millimeter-wave fan-beam antenna based on step-index cylindrical homogeneous lens," *IEEE Antennas Wireless Propag. Lett.*, vol. 11, pp. 1512–1516, 2012.
- [30] O. Lafond, M. Himdi, H. Merlet, and P. Lebars, "An active reconfigurable antenna at 60 GHz based on plate inhomogeneous lens and feeders," *IEEE Trans. Antennas Propag.*, vol. 61, no. 4, pp. 1672–1678, Apr. 2013.
- [31] A. S. Gutman, "Modified Luneberg lens," *J. Appl. Phys.*, vol. 25, no. 7, pp. 855–859, Jul. 1954, doi: [10.1063/1.1721757](https://doi.org/10.1063/1.1721757).
- [32] O. Zetterstrom, N. J. G. Fonseca, and O. Quevedo-Teruel, "Additively manufactured half-gutman lens antenna for mobile satellite communications," *IEEE Antennas Wireless Propag. Lett.*, vol. 22, pp. 759–763, 2023, doi: [10.1109/LAWP.2022.3224455](https://doi.org/10.1109/LAWP.2022.3224455).
- [33] P. Bantavis, C. G. Gonzalez, C. Diallo, R. Sauleau, G. Goussetis, S. Tubau, and H. Legay, "All-metal graded index Gutman lens antenna—A more compact Luneburg lens," in *Proc. 14th Eur. Conf. Antennas Propag. (EuCAP)*, Copenhagen, Denmark, Mar. 2020, pp. 1–4, doi: [10.23919/EuCAP48036.2020.9135859](https://doi.org/10.23919/EuCAP48036.2020.9135859).
- [34] O. Bjorkqvist, O. Zetterstrom, and O. Quevedo-Teruel, "Additive manufactured dielectric Gutman lens," *Electron. Lett.*, vol. 55, no. 25, pp. 1318–1320, Dec. 2019, doi: [10.1049/el.2019.2483](https://doi.org/10.1049/el.2019.2483).
- [35] S. Biswas and M. S. Mirotznik, "Customized shaped Luneburg lens antenna design by additive fabrication," in *Proc. 18th Int. Symp. Antenna Technol. Appl. Electromagn. (ANTEM)*, Aug. 2018, pp. 1–2.
- [36] Z. Larimore, S. Jensen, P. Parsons, B. Good, K. Smith, and M. Mirotznik, "Use of space-filling curves for additive manufacturing of three dimensionally varying graded dielectric structures using fused deposition modeling," *Additive Manuf.*, vol. 15, pp. 48–56, May 2017.
- [37] S. Biswas and M. Mirotznik, "High gain, wide-angle QCTO-enabled modified Luneburg lens antenna with broadband anti-reflective layer," *Sci. Rep.*, vol. 10, no. 1, pp. 1–20, Jul. 2020.
- [38] S. Biswas, "Dual-polarized antenna feed matrix design for multi-beam lens antenna," *IEEE Antennas Wireless Propag. Lett.*, vol. 22, pp. 2760–2764, 2023, doi: [10.1109/LAWP.2023.3308824](https://doi.org/10.1109/LAWP.2023.3308824).



- [39] C. Wang, J. Wu, and Y.-X. Guo, "A 3-D-Printed multibeam dual circularly polarized Luneburg lens antenna based on quasi-icosahedron models for Ka-band wireless applications," *IEEE Trans. Antennas Propag.*, vol. 68, no. 8, pp. 5807–5815, Aug. 2020, doi: 10.1109/TAP.2020.2983798.
- [40] M. Imbert, J. Romeu, and L. Jofre, "Dielectric flat lenses with cylindrically distributed parameters for millimeter-wave applications," in *Proc. 10th Eur. Conf. Antennas Propag.*, 2016, pp. 1–5.
- [41] J. Pourahmadazar and T. A. Denidni, "Multi-beam tapered slot antenna array using substrate integrated waveguide Rotman lens," in *Proc. Eur. Radar Conf.*, 2015, pp. 425–428.
- [42] P. Chen, W. Hong, Z. Kuai, and J. Xu, "A double layer substrate integrated waveguide Blass matrix for beamforming applications," *IEEE Microwave Wireless Compon. Lett.*, vol. 19, no. 6, pp. 374–376, Jun. 2009, doi: 10.1109/LMWC.2009.2020020.



**MIAO LV** received the B.S. degree in electronic information engineering and the M.S. degree in electromagnetic wave and microwave technology from Xidian University, Xi'an, China, in 2011 and 2014, respectively, where he is currently pursuing the Ph.D. degree with National Key Laboratory of Radar Detection and Sensing.

Since 2020, he has been a Senior Engineer with the 20th Research Institute of China Electronics Technology Group Corporation. His research interests include phased array antennas, metamaterial antennas, and reconfigurable antennas.



**LI ZHANG** received the B.S. and M.S. degrees in electromagnetic wave and microwave technology from Xidian University, Xi'an, China, in 2011 and 2014, respectively, where he is currently pursuing the Ph.D. degree with National Key Laboratory of Radar Detection and Sensing.

He is working in the 20th Research Institute of China Electronics Technology Group Corporation. His research interests include phased array antenna, mm-wave antenna, and in-band full-duplex antenna.



**MENGYI LI** was born in Shanxi, China, in 2001. She received the B.S. degree in electronic information engineering, in 2023. She is currently pursuing the M.S. degree with National Key Laboratory of Radar Detection and Sensing, Xidian University.

Her main research interest includes lens antennas.



**FANCHAO ZENG** (Graduate Student Member, IEEE) was born in Shandong, China, in 1995. He received the B.Eng. and M.Eng. degrees from the School of Electronic Engineering, Xidian University, Xi'an, China, in 2018 and 2021, respectively. He is currently pursuing the Ph.D. degree with the Global Big Data Technologies Centre (GBDTC), University of Technology Sydney (UTS), Sydney, NSW, Australia. His current research interests include antenna array, antenna polarization, base station antennas, mm-wave antennas, and Mie-scattering.



**SHAOLI ZUO** was born in Shaanxi, China, in 1985. She received the B.S. degree in electrical engineering and the Ph.D. degree in electromagnetic field and microwave technology from Xidian University, Xi'an, China, in 2007 and 2012, respectively. She is currently with the National Key Laboratory of Radar Detection and Sensing, Xidian University. Her current research interests include broadband antennas and antenna arrays.



**ZHI-YA ZHANG** was born in Jiangsu, China, in 1985. He received the B.S. degree in electrical engineering and the Ph.D. degree in electromagnetic field and microwave technology from Xidian University, Xi'an, China, in 2007 and 2012, respectively. He is currently a Professor with the National Key Laboratory of Radar Detection and Sensing, Xidian University. His current research interests include broadband antennas, millimeter-wave antennas, and antenna arrays.



**YU WANG** received the B.S. degree in electricity and electronic engineering from Xidian University, Xi'an, China, and the M.S. degree in microwave engineering from Xidian University, and Doshisha University, Kyoto, Japan, in 2012. He works in the 20th Research Institute of China Electronics Technology Group Corporation and CETC Key Laboratory of Data Link Technology.



**TONG WU** was born in Jiangsu, China, in 1994. He is currently pursuing the Ph.D. degree in electronic science and technology with the National Key Laboratory of Radar Detection and Sensing, Xidian University. His current research interests include tightly coupled array antenna, and antenna array theory and its isolation technology.

...